Preparation and Nucleation Study of β-PbO₂-WC Composite Coating Electrode for Oxygen Evolution Reaction

Shiwei He[1,2], *Ruidong Xu*[3], *Bohao Yu*[3], *Yuqing Guo*[4], *Zhongsheng Hua*[2,*], *Fuyuan Zhang*[2], *Huihong Lv*[1]

[1] Key Laboratory of Metallurgical Emission Reduction & Resources Recycling, Ministry of Education, Maanshan, 243002, China
[2] School of Metallurgical Engineering, Anhui University of Technology, Maanshan 243002, China
[3] State Key Laboratory of Complex Nonferrous Metal Resources Cleaning Utilization, Kunming, 650093, China
[4] College of Chemistry, Chemical Engineering and Biotechnology, Donghua University, Shanghai, 201620, China
[*]E-mail: ahutyouse01@163.com

In this study, β-PbO₂-WC composite coatings were synthesized on a substrate using the electrodeposition method in an electrolyte containing Pb^{2+} and WC particles. The preparation process study shows that the β-PbO₂ bath containing WC particles becomes more stable for an ultrasonic dispersion time within 30 minutes. WC particles in the β-PbO₂ bath are positively charged, with anions being adsorbed onto the particles. Compared to the β-PbO₂ composite electrode, the oxygen evolution overpotentials for the β-PbO₂-WC electrode are decreased, which demonstrates an energy-saving effect. The nucleation behavior study shows that the co-deposition of WC particles into the layer has little effect on the crystal growth of β-PbO₂. The main process during the deposition time of 0~5 min were the nucleation of the β-PbO₂ grains, the adsorption of WC particles, growth of β-PbO₂ grains, and WC particles coated.

1. INTRODUCTION

The oxygen evolution reaction (OER) is an important reaction in modern industry. This reaction plays an important role in hydrogen production, electro-organic syntheses, and metal electrowinning processes. OER requires the distribution of four redox processes: the coupling of multiple proton and electron transfers, and the formation of two O-O bonds[1]. In an electrochemical

system, OER occurs at high positive potentials when water solution is used as the electrolyte. When OER is the primary reaction at the anode, a large amount of the energy in the electrochemical system will be dedicated to it. Therefore, the continued development of catalysts to improve OER efficiency remains a central scientific and technological challenge.

Coated electrodes are now extensively used in the electrochemical field because they have both the mechanical properties of the substrate and the electrochemical properties of the coating. As one of the more traditional coatings, lead dioxide (PbO_2) has attracted considerable attention due to its demonstrated advantages, including low electrical resistivity, low cost, ease of preparation, good chemical stability, and relatively large surface area[2-5]. Thus, lead dioxide has already been used in waste water treatment[6-8], ozone generation[9,10], lead-acid batteries[11-13], analytical sensors[14], and the metal electrowinning process[15]. It is well-known that PbO_2 shows two phases: the α phase and β phase. Electrodeposition is a traditional way to prepare these two phases of PbO_2[16]. The conditions (primarily composition and temperature) of the synthesizing bath determine the phase of the deposited material[17]. To the best of our knowledge, the electrochemical activity and electrical conductivity of β-PbO_2 is better than that of α-PbO_2[18]. However, as an interlayer of the electrode, the binding force for β-PbO_2 and its underlayer can be improved by using α-PbO_2[19].

The OER is sensitive to the intrinsic structure of the catalysts[20]. WC is an excellent electrocatalytic substance, and it exhibit a similar electrocatalytic effect like platinum. Due to its high hardness (close to the diamond), good electrical and thermal conductivity, WC has been widely used for cemented carbide, catalysis and fuel cells[21-25]. WC doping into the PbO_2 matrix will improve the mechanical properties for the composite deposit and refine the grain structure for the PbO_2 deposit[26,27]. In addition, some researchers also found that WC particle-doped PbO_2 anodes have lower oxygen evolution overpotentials and stronger corrosion resistance in acidic systems compared to pure PbO_2 anodes [28] .

In this study, the β-PbO_2-WC composite coatings were synthesized on the substrate by the electrodeposition method in the electrolyte containing Pb^{2+} and WC particles. In order to improve the binding force of the substrate and the β-PbO_2-WC out layer, the substrates were covered with an α-PbO_2 layer by electrodeposition pretreatment. The influences of composite coating preparation parameters, such as ultrasonic dispersion time and particle concentration of the electrolyte, have been investigated using Zeta potential test and anodic polarization test. The morphology and structure of the β-PbO_2-WC composite layer in different nucleation time was measured by means of XRD, SEM, EDS. To the best of our knowledge, the nucleation process of the β-PbO_2-WC composite on the surface of the α-PbO_2 layer has never been studied so meticulously.

2. EXPERIMENTATION

2.1. Materials and reagents

Pb-0.3%Ag alloy plate with dimension of 40 mm×20 mm×2 mm was selected as the substrate. All chemicals were of analytical grade and purchased from Aladdin Industrial Corporation (Shanghai, China). All solutions were prepared by deionized water from an EPED water purification system. Bath

solutions were prepared by dissolving $Pb(NO_3)_2$ in HNO_3 solution. The concentrations of Pb^{2+} and HNO_3 were controlled at 0.8 M and 0.2 M, respectively.

2.2. Electrode preparation

The β-PbO_2-WC composite electrode (Pb-0.3%Ag/α-PbO_2/β-PbO_2-WC) consisted of Pb-0.3%Ag alloy substrate, α-PbO_2 inter layer, and β-PbO_2-WC outer layer. Firstly, the Pb-0.3%Ag alloy substrates were pretreated by polishing, degreasing, and acid etching. Secondly, the α-PbO_2 inter layer was electrodeposited in alkaline solution which consisted of 3 M NaOH and 0.15 M Pb(II). The current density and temperature was controlled at 13.5 mA/cm^2 and 40°C, respectively. The β-PbO_2 plating bath was consisted of 0.2 M HNO_3+0.8 M Pb^{2+} with different concentration of WC particle. The β-PbO_2 composite electrode (Pb-0.3%Ag/α-PbO_2/β-PbO_2) was obtained in the electrolyte without WC particle (concentration of WC particle is 0g/L). Figure 1 is the schematic diagram of the electrode preparation device. The substrate was contacted with anode and the stainless steel plates were contacted with cathode.

2.3. Zeta potential and particle size test

The zeta potential and particle size was measured by analyzing WC(0.1 g) in solution(10 ml) using the ZetaPALS (Brookhaven). All samples were sonicated for 0~50 minutes before Zeta potential measurements. The frequency and power of the ultrasonicator was controlled at 40 kHz and 300 W, respectively. The zeta potential was measured from the electrophoretic mobility by the Smoluchowski equation.

2.4. Anodic polarization curve measurement

The anodic polarization curves were obtained in a synthetic zinc electrowinning simulated electrolyte of 50g/L Zn^{2+} (added as $ZnSO_4$) and 150 g/L H_2SO_4, at 35 °C. The scan rates were controlled at 5 mV/s. All the electrochemical measurements were conducted by PARSTAT2273 electrochemical workstation with a three-electrode system. The working electrode, which effective area was 1 cm^2, was firstly dealt with wax-sealing. The reference electrode was saturated calomel electrode (SCE) and the counter electrode was graphite electrode. The reference electrode and working electrode were linked by luggin capillary filled with agar and potassium chloride. In addition, the distance between capillary and working electrode surface was about 2d (d is the diameter of capillary), and d was 0.5 mm.

2.3. Characterization of surface and phase composition

The phase composition and surface microstructure characteristics of PbO_2 composite layer were measured by D/Max-2200 X-ray diffractometer (XRD) and Nova NanoSEM450 scanning electron microscope (SEM), respectively.
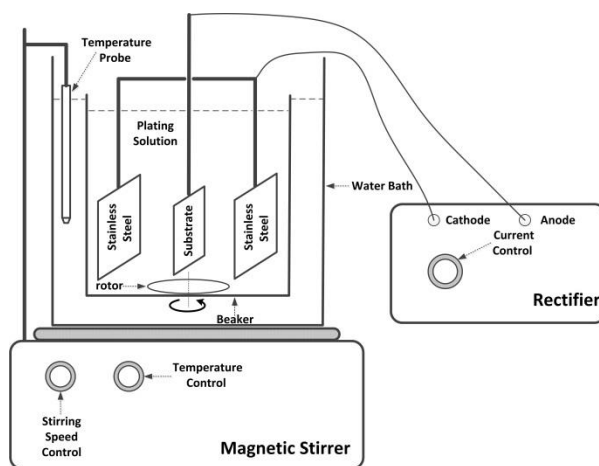
Figure 1. Schematic diagram of the electrode preparation device

3. RESULTS AND DISCUSSION

3.1. Preparation of the electrode

The Zeta potential and particle size measured in a solution of 0.2 M HNO_3+0.8 M Pb^{2+} with varying WC particle concentrations are shown in Fig. 1. The measured particle size was reduced from 0.87 μm to 0.71 μm for an ultrasonic dispersion time of 20 minutes, which indicates a significant decrease. Following this decrease, the particle size was stabilized at approximately 0.71 μm. This phenomenon is observed because the particles with larger size gradually sank to the bottom of the containing vessel in the first 20 minutes.
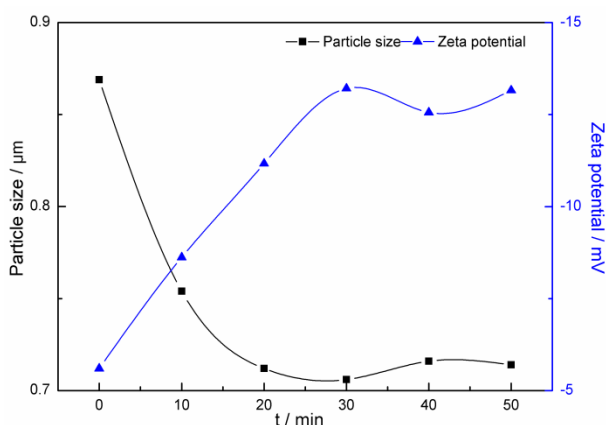
Figure 2. Particle size and Zeta potential for WC particles in a β-PbO$_2$ plating bath at different ultrasonic dispersion times

The blue line shows the Zeta potential value along with the ultrasonic dispersion time. The Zeta potential value for the WC particles in this solution gradually increased from 0 to 30 min. When the ultrasonic dispersion time exceeded 30 min, the value for the Zeta potential changes little. The absolute value of the Zeta potential is mainly used to characterize the stability of the solution. A greater

absolute value for the Zeta potential indicates a more stable solution[29,30]. Therefore, the β-PbO$_2$ bath containing WC particles becomes more stable for an ultrasonic dispersion time within 30 minutes. In addition, the Zeta potential values are negative in all the ultrasonic time ranges, indicating that WC particles are positively charged and that anions are adsorbed onto the particles. Considering the variation law for the particle size and Zeta potential with ultrasonic time, an ultrasonic dispersion time of 30 min is more suitable.

The WC doped β-PbO$_2$ electrodes were prepared in β-PbO$_2$ baths with different WC particle concentrations(0~40 g/L). The ultrasonic dispersion time for the β-PbO$_2$ baths were controlled at 30 min. In addition, the temperature and time of the deposition process was controlled at 45 ℃ and 1 hour, respectively. The anodic polarization curves for the β-PbO$_2$-WC composite electrodes measured in a Zn electrowinning simulated system are shown in Fig. 3. As shown in Fig. 3, the characteristics for the five anodic polarization curves are similar, with the current being almost zero before oxygen evolution and exponentially increasing after oxygen evolution, which are typical OER characteristic curves. With the doping of WC particles, the initial oxygen evolution potentials for the electrodes were significantly reduced compared with the β-PbO$_2$ electrodes without particles. Furthermore, the initial oxygen evolution potential shows a decreasing trend as the concentration of WC increases in the β-PbO$_2$ plating bath. When the WC concentration in the solution is 30 g/L and 40 g/L, the initial oxygen evolution potential is smaller and close.
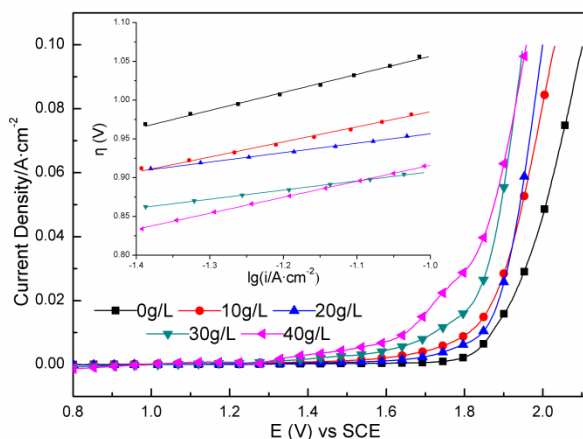
Figure 3. Anodic polarization curves for β-PbO$_2$-WC composite electrodes in a simulation zinc electrowinning solution obtained from the original plating bath with different WC concentrations

The inset in Fig. 3 shows the Tafel lines (η=a+blgi) in the OER potential range. The kinetic parameters for the Tafel linear fitting and OER overpotential at a current density of 300, 400, 500 and 600 mA/cm^2 are shown in Table 1. It can be found from Table 1 that the Tafel intercept (a) and the Tafel slope (b) are significantly reduced as the WC particles are doped into the electrode. Both the Tafel intercept (a) and the Tafel slope (b) showed a decreasing first and then increasing trend. When the concentration of WC particles in the original solution was 30 g/L, the values of the Tafel intercept (a) and the Tafel slope (b) were the smallest, 1.025 and 0.118, respectively. A smaller Tafel slope is more beneficial for energy-saving as it leads to a remarkably increased OER rate with an increase in overpotential[31-33]. When the WC particle concentration in the plating bath is 30 g/L,

the oxygen evolution overpotentials calculated at the different current densities were the lowest for the obtained electrode. Compared to the electrode prepared without WC particles, the oxygen evolution overpotentials for the electrode at 300 A/m^2, 400 A/m^2, 500 A/m^2 and 600 A/m^2 are decreased by 89 mV, 103 mV, 115 mV, and 123 mV, respectively, which indicates an energy-saving effect.

Table 1. Kinetic parameters and overpotential for the OER at β-PbO$_2$-WC composite electrodes in a simulation zinc electrowinning solution obtained from the original plating bath with varying WC concentration

WC concentration g/L	Oxygen evolution overpotential η / V				a	b	i^0 / A·cm^{-2}
	300A·m^{-2}	400A·m^{-2}	500A·m^{-2}	600A·m^{-2}			
0 (β-PbO$_2$)	0.934	0.963	0.986	1.004	1.289	0.233	2.94×10^{-6}
10	0.884	0.908	0.927	0.942	1.179	0.194	8.37×10^{-7}
20	0.892	0.907	0.919	0.929	1.078	0.122	1.46×10^{-9}
30	0.845	0.860	0.871	0.881	1.025	0.118	2.06×10^{-9}
40	0.808	0.834	0.854	0.870	1.122	0.206	3.58×10^{-6}

The kinetic parameters for different composite electrodes are shown in Table 2. Pb-0.3%Ag/α-PbO$_2$/β-PbO$_2$ is the electrode that was prepared with the WC concentration of 0 g/L in Table 1. Pb-0.3%Ag/α-PbO$_2$/β-PbO$_2$-WC is the electrode that was prepared with the WC concentration of 30 g/L, which was possess best energy saving effect for OER (from Table 1). The other electrodes were discussed from the reference[34,35]. The OER overpotential (η) for Pb-0.3%Ag/Pb-WC and Pb-0.3%Ag/Pb-CeO$_2$ electrodes are decreased, compared to Pb-0.3%Ag electrode. It indicate that the fabrication of Pb-WC and Pb-CeO$_2$ layer on the Pb-0.3%Ag substrate can improve the OER energy-saving effect for the electrodes. In addition, the OER overpotential (η) for Pb-0.3%Ag/α-PbO$_2$/β-PbO$_2$-WC electrode is much lower than Pb-0.3%Ag/Pb-WC electrode, which indicate that the β-PbO$_2$-WC composite layer with an α-PbO$_2$ interlayer exhibited better energy-saving effect for OER than the Pb-WC layer, as both synthesized on the Pb-0.3%Ag substrate.

Table 2. Kinetic parameters and overpotential for the OER at different composite electrodes in a simulation zinc electrowinning solution obtained from the original plating bath

Electrode type	Oxygen evolution overpotential η / V			a	b	i^0 / A·cm^{-2}
	400A·m^{-2}	500A·m^{-2}	600A·m^{-2}			
Pb-0.3%Ag/α-PbO$_2$/β-PbO$_2$	0.963	0.986	1.004	1.289	0.233	2.94×10^{-6}
Pb-0.3%Ag/α-PbO$_2$/β-PbO$_2$-WC	0.860	0.871	0.881	1.025	0.118	2.06×10^{-9}
Pb-0.3%Ag/Pb-WC[34]	/	0.926	0.94	1.275	0.335	1.65×10^{-7}
Pb-0.3%Ag/Pb-CeO$_2$[35]	1.119	1.134	1.147	1.336	0.155	2.41×10^{-9}
Pb-0.3%Ag[35]	1.207	1.22	1.231	1.401	0.139	8.33×10^{-11}

3.2. Nucleation of the composite layer

The substrates in this section are Pb-0.3%Ag/α-PbO$_2$, and all the studies on the nucleation process are on the surface of α-PbO$_2$ interlayer. In the nucleation study, the β-PbO$_2$-WC compostie electrodes were prepared in β-PbO$_2$ bath with a WC particle concentration of 30 g/L. The β-PbO$_2$-WC compostie electrodes obtained from six different electrodeposition times of 0 s, 10 s, 30 s, 2 min, 5 min and 60 min. The XRD patterns of the β-PbO$_2$-WC compostie electrodes prepared with or without WC particles are shown in Figure 4. Fig. 5~Fig. 7 shows the SEM images and EDS analysis of the β-PbO$_2$-WC compostie electrodes prepared at different electrodeposition times.
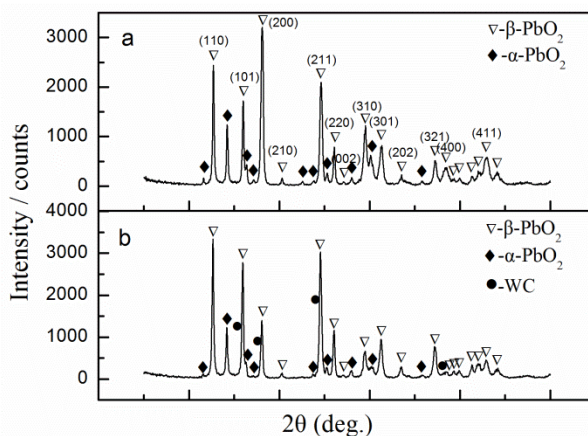
Figure 4. The XRD patterns of β-PbO$_2$ composite electrode (a) and β-PbO$_2$-WC composite electrode (b)

It can be seen from the pattern (a) of the Fig. 4 that the PbO$_2$ electrodeposited in the acidic solution is mainly composed of the β phase[36,37], but still contains small amount of the α phase. Comparing the pattern (a) and (b), it can be found that the peak position and intensity for the two patterns are almost consistent, which indicates that the co-deposition of WC particles into the layer has little effect on the crystal growth of β-PbO$_2$. Table 3 shows the elements content of β-PbO$_2$-WC composite layer. The content of W is 2.59wt%, so that the content of WC in the composite layer can be calculated. The calculated value of WC content is 2.76wt%.

Table 3. The elements content of β-PbO$_2$-WC composite layer

Element	W	Pb
Content (wt%)	2.59	82.74
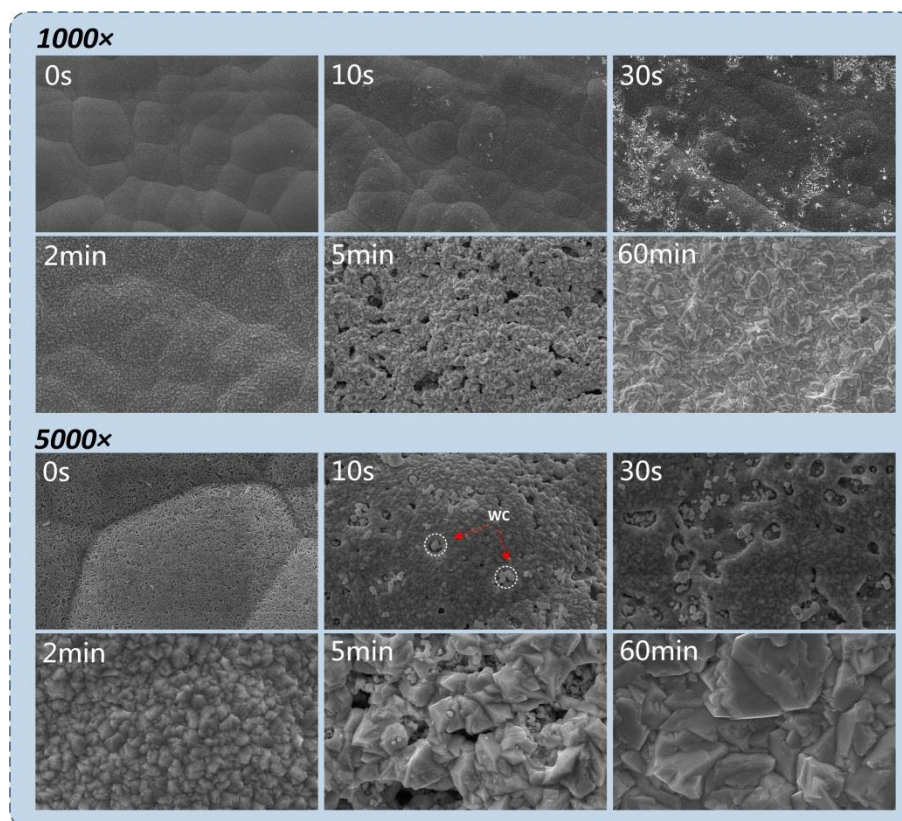
Figure 5. The SEM images of β-PbO$_2$-WC compostie electrodes obtained at different deposition time (1000×, 10000×)

It can be seen from Fig. 5 that the morphology of the substrate is presented, when the deposition time was 0 s. The α-PbO$_2$ substrate is composed of circular cells, the circular cell boundaries is clear, and the cell is consisted of interwoven rod-shaped crystal grains.

When the deposition time was 10 s, the circular shape of the α-PbO$_2$ substrate is still visible, but a layer of β-PbO$_2$ nucleus has formed on the surface. In addition, some WC particles have been adsorbed on the surface of the sediment layer. The preferentially adsorbed positions of WC particles were random. It can be concluded that the main process during the deposition time of 0~10 s were the nucleation of the β-PbO$_2$ grains and the adsorption of WC particles.

When the deposition time was 30 s, the circular shape of α-PbO$_2$ is still visible. And the β-PbO$_2$ crystal grains have completely covered the surface of the substrate and begin to grow. In addition, more WC particles have been adsorbed on the surface. It is indicated that the main process during the deposition time of 10~30 s were the growth of β-PbO$_2$ grains on the substrate and the adsorption of WC particles.

When the deposition time was 2 min, the circular shape of α-PbO$_2$ is still visible, and the β-PbO$_2$ crystal grains continue to grow. Moreover, the grain size of β-PbO$_2$ was significantly larger than the grain under the deposition time of 30 s. It shows that in the deposition time of 30 s~2 min, the main process at the electrode was the growth of β-PbO$_2$ crystal grains on the substrate.
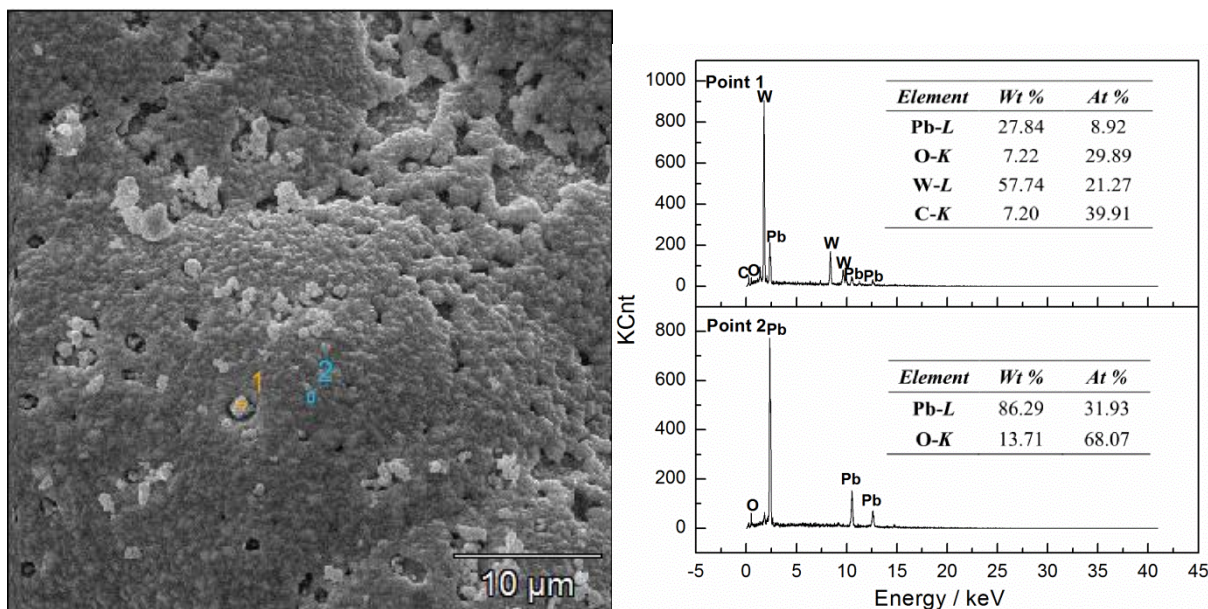
Figure 6. Energy spectrum analysis for the β-PbO₂-WC compostie electrode for 10 s of electrodeposition
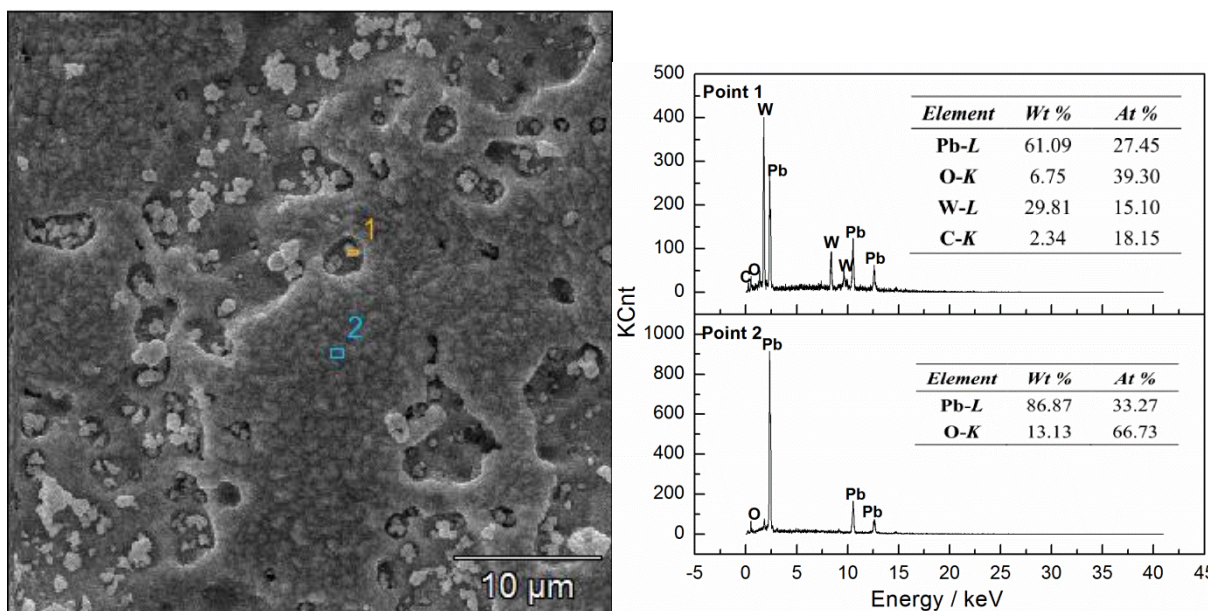
Figure 7. Energy spectrum analysis for the β-PbO₂-WC compostie electrode for 30 s of electrodeposition

When the deposition time was 5 min, the circular shape of the α-PbO₂ substrate has basically disappeared, and the grain size of β-PbO₂ on the substrate grows obviously. It shows that in the deposition time of 2~5 min, the main process at the electrode was the growth of β-PbO₂ crystal grains on the substrate.

When the deposition time was extended to 60 min, the grain size of β-PbO₂ on the substrate continuously increased, and the WC particles were totally covered by β-PbO₂ grains. This shows that

in the deposition time of 5 to 60 minutes, the main process at the electrode were the continuously growth of β-PbO$_2$ grains on the substrate, and the WC particles coated.

From Fig. 6 and Fig. 7, point 1 in both two figures is positioned on the WC particles, and the point 2 in both two figures is positioned on the PbO$_2$ grains, respectively. The Pb and O content of point 1 in Fig.7 is higher than point 1 in Fig.6. This indicate that PbO$_2$ film covered on the WC particles become thicker, when the deposition time was extended from 10 s to 30 s.

Based on the previous analysis, the nucleation process for the β-PbO$_2$-WC deposition layer can be divided into four steps: step 1: the WC particles suspended in the β-PbO$_2$ plating bath move from the depth of the plating solution to the vicinity of the substrate surface depending on the flow of the plating solution. Step 2: nucleation of β-PbO$_2$ on the substrate starts at the α-PbO$_2$ substrate. The second step and the first step do not have a sequence and can be performed at the same time. Step 3: the WC particles with anionic absorbents are electrophoretically pushed to the surface of the anode and adsorbed on the surface of the anode after reaching the double layer of the anode surface. Step 4: the β-PbO$_2$ on the substrate continues to grow. At the same time, β-PbO$_2$ nucleates on the adsorbed WC particles, resulting in gradual but complete coating of the WC particles with β-PbO$_2$.

4. CONCLUSIONS

In this study, the stability of a WC suspension electrolyte was investigated by a Zeta potential test. The β-PbO$_2$ bath containing WC particles becomes more stable for an ultrasonic dispersion time within 30 minutes. The Zeta potential values are negative in all the ultrasonic time ranges, indicating that WC particles are positively charged and that anions are adsorbed onto the particles.

The influence of the WC concentration on the electrode OER catalytic properties was characterized using anodic polarization curves. The oxygen evolution overpotential for the obtained electrode was the lowest for a WC particle concentration of 30 g/L in the plating bath. Compared to the β-PbO$_2$ composite electrode, the oxygen evolution overpotentials for the electrode at 300 A/m^2, 400 A/m^2, 500 A/m^2 and 600 A/m^2 are decreased by 89 mV, 103 mV, 115 mV, and 123 mV, respectively, which demonstrates an energy-saving effect.

XRD, SEM, and EDS were utilized to investigate the nucleation of the composite layer. The co-deposition of WC particles into the layer has little effect on the crystal growth of β-PbO$_2$. The main process during the deposition time of 0~10 s were the nucleation of the β-PbO$_2$ grains and the adsorption of WC particles. The main process during the deposition time of 10~30 s were the growth of β-PbO$_2$ grains on the substrate and the adsorption of WC particles. The main process during the deposition time of 30 s~5 min was the growth of β-PbO$_2$ crystal grains on the substrate. In addition, the main process during the deposition time of 5 to 60 minutes were the continuously growth of β-PbO$_2$ grains on the substrate and the WC particles coated.

References

1. M. Tahir, L. Pan, F. Idrees, X. Zhang, L. Wang, J. J. Zou, and Z. L. Wang, *Nano Energy*, 37 (2017) 136.
2. A. M. Couper, D. Pletcher, and F. C. Walsh, Cheminform abstract: electrode materials for electrosynthesis, *Cheminform*, 21 (1990) 837.
3. S. He, R. Xu, S. Han, J. Wang, and B. Chen, *Int. J. Electrochem. Sci.*, 11 (2016) 5245.
4. M. Panizza, I. Sirés, and G. Cerisola, *J. Appl. Electrochem.*, 38 (2008) 923.
5. L. Chang, Y. Zhou, X. Duan, W. Liu, and D. Xu, *J. Taiwan Inst. Chem. E.*, 45 (2014) 1338.
6. D.C. Johnson, J. Feng, and L.L. Houk, *Electrochim. Acta*, 46 (2000) 323.
7. H. An, Q. Li, D. Tao, H. Cui, X. Xu, L. Ding, and J. Zhai, *Appl. Surf. Sci.*, 258 (2011) 218.
8. J. Xing, D. Chen, W. Zhao, X. Zhao, and W. Zhang, *RSC Adv.*, 66 (2015) 53504.
9. R. Amadelli, L. Armelao, A.B. Velichenko, N.V. Nikolenko, D.V. Girenko, S.V. Kovalyov, and F.I. Danilov, *Electrochim. Acta*, 45 (1999) 713.
10. J. Wu, H. Xu, and W. Yan, *RSC Adv.*, 25 (2015) 19284.
11. H.Y. Chen, L. Wu, C. Ren, Q.Z. Luo, Z.H. Xie, X. Jiang, and Y.R. Luo, *J. Power Sources*, 95 (2001) 108.
12. A. Moncada, M.C. Mistretta, S. Randazzo, S. Piazza, C. Sunseri, and R. Inguanta, *J. Power Sources*, 256 (2014) 72.
13. A. Moncada, S. Piazza, C. Sunseri, and R. Inguanta, *J. Power Sources*, 275 (2015) 181.
14. D. Velayutham, and M. Noel, *J. Appl. Electrochem.*, 23 (1993) 922.
15. C.J. Yang, and S.M. Park, *Electrochim. Acta*, 108 (2013) 86.
16. H. Bode, Lead-Acid Batteries, Wiley, New York, 1977.
17. D. Devilliers, T. Dinh, E. Mahé, V. Dauriac, and N. Lequeux, *J. Electroanal. Chem.*, 573 (2004) 227.
18. B. Chen, Z. Guo, H. Huang, X. Yang, and Y. Cao, *Acta Metall. Sin.*, 22 (2009) 373.
19. S. He, R. Xu, G. Hu, and B. Chen, *Electrochemistry*, 83 (2015) 974.
20. B. M. Jović, U. Č. Lačnjevac, V. D. Jović, and N. V. Krstajić, *J. Electroanal. Chem.*, 754 (2015) 100.
21. R. B. Levy, and M. Boudart., *Science*, 181 (1973) 547.
22. D. R. Mcintyre, G. T. Burstein, and A. Vossen, *J. Power Sources*, 107 (2002) 67.
23. Y. Oh, S. K. Kim, D. H. Peck, J. S. Jang, J. Kim, and D. H. Jung, *Int. J. Hydrogen Energy*, 39 (2014) 15907.
24. P. K. Sahoo, S. S. K. Kamal, M. Premkumar, T. J. Kumar, B. Sreedhar, and A. K. Singh, *Int. J. Refract Met. Hard. Mater.*, 27 (2009) 784.
25. L. He, Y. Tan, X. Wang, H. Tan, and C. Zhou, *Surf. Coat. Technol.*, 244 (2014) 123.
26. Z. A. Hamid, I. M. Ghayad, and K. M. Ibrahim, *Surf. Interface Anal.*, 37 (2005) 573.
27. Y. Boonyongmaneerat, K. Saengkiettiyut, S. Saenapitak, and S. Sangsuk, *Surf. Coat. Tech.*, 203 (2009) 3590.
28. L. Huixi, C. Zhen, Y. Qiang, Z. Wei, and C. Wenrong, *J. Electrochem. Soc.*, 164 (2017) H1064.
29. R. Marsalek, *Apcbee Procedia*, 9 (2014) 13.
30. X. Tang, H. Zheng, H. Teng, C. Zhao, Y. Wang, W. Xie, W. Chen, and C. Yang, *Eng. Res. Des.*, 104 (2015) 208.

31. Z. Li, X. Y. Yu, and U. Paik, *J. Power Sources*, 310 (2016) 41.
32. X. Song, T. Yang, H. Du, W. Dong, and Z. Liang, *J. Electroanal. Chem.*, 760 (2016) 59.
33. M. Abreu-Sepulveda, P. Trinh, S. Malkhandi, S. R. Narayanan, J. Jorné, D. J. Quesnel, and A. Manivannan, *Electrochim. Acta*, 180 (2015) 401.
34. S. He, R. Xu, J. Wang, S. Han, and B. Chen, *J. Wuhan Unive. Technol.*, 31 (2016) 811.
35. S. He, R. Xu, H. Chen, L. Huang, Y. Kong, and B. Chen, *Rare Metal Mat. Eng.*, 43 (2014) 1917.
36. I. Petersson, E. Ahlberg, and B. Berghult, J. Power Sources, 76(1998) 98.
37. R. Amadelli, A. Maldotti, A. Molinari, F. I. Danilov, and A. B. Velichenko, J. Electroanal. Chem., 534(2002)1.